Journal of Materials Chemistry A

A Comparative Study on the Oxidation of Two-Dimensional Ti3C2 MXene Structures in Different Environments

Journal:	*Journal of Materials Chemistry A*
Manuscript ID	TA-ART-02-2018-001468.R1
Article Type:	Paper
Date Submitted by the Author:	14-May-2018
Complete List of Authors:	Lotfi, Roghayyeh; Penn State University, ; Roghayyeh Lotfi, Naguib, Michael; Drexel University, Department of Materials Science and Engineering; Drexel University, A. J. Drexel Nanomaterials Institute Yilmaz, Dundar; Penn State Nanda, Jagjit; oak ridge national laboratory, Materials Science & Technology Divison van Duin, Adri; The Pennsylvania State University, Mechanical and Nuclear Engineering

A Comparative Study on the Oxidation of Two-Dimensional Ti_3C_2 MXene Structures in Different Environments

Roghayyeh Lotfi[a], Michael Naguib[b], Dundar E. Yilmaz[a], Jagjit Nanda,[b] Adri C. T. van Duin [*a]

Abstract

Oxidation of two-dimensional Ti_3C_2 MXene structure has been recognized as a promising method for the formation of hybrid structures of carbon supported nano titania. Here, we studied the oxidation of Ti_3C_2 MXene structure using reactive force field (ReaxFF) based molecular dynamics simulations. To investigate the effect of oxidation agent, we used three different environments including dry air (oxygen molecules), wet air (oxygen and water molecules) and hydrogen peroxide (H_2O_2 molecules). Oxidation simulations were performed at different temperatures of 1000, 1500, 2000, 2500 and 3000 K. We found that by controlling the temperature, carbon supported titania can be formed by diffusion of Ti atoms to the surface of MXene structure during the oxidation. These results were confirmed by increase in the average bond orders of C-C and Ti-O and decrease in the average bond orders of Ti-C. Moreover, it was revealed that by increasing the temperature, the oxidation rate increases, and the rate depends on

[a] *Department of Mechanical and Nuclear Engineering, The Penn State University, University Park, PA 16802, USA. *Email: acv13@psu.edu*

[b] *Materials Science and Technology Division, Oak Ridge National Laboratory, Oak Ridge, TN 37831, USA*

the oxidant according to the following order in: H_2O_2 > wet air > dry air. This was validated by heating MXene in wet air and dry air followed by examining the products using X-ray diffraction and Raman spectroscopy. To investigate the effect of presence of oxidant, MXene structure was also heated under vacuum, and it was found that in this case the MXene structure was converted to cubic TiC. Furthermore, it was indicated that during the heating process of MXene structure in the vacuum, the average bond orders for C-C, Ti-C and Ti-O do not change significantly due to the lack of oxidants in the environment, leaving room for only topotactic transformation of atoms during the heating. Formation of TiC structure by heating MXene in an inert environment was confirmed experimentally as well.

1. Introduction

Two-dimensional (2D) materials possess unique electronic, optical and chemo-mechanical properties, which have attracted extensive attraction during the past decade.[1-5] Graphene, hexagonal boron nitrides, metal chalcogenides are some examples of 2D materials which have been widely studied.[5-7] Recently, a new family of 2D materials, transition metal carbides, carbonitrides and nitrides refereed as "MXenes", has been discovered. MXenes are usually synthesized by selective etching of A (mostly Al or Ga) layers from MAX phase; where M is an early transition metal (e.g. Ti, V, Cr, Mo, and Nb), and X is carbon and/or nitrogen[8]; by using fluoride containing aqueous solution.[9] The general formula for MXene structures is $M_{n+1}X_nT_x$ (n=1-3), in which T_x is the terminating functional group (O, OH or F).[10-13] Due to superior properties of MXenes, these novel 2D materials have found diverse applications in energy storage including lithium ion batteries (LIBs), electrode materials and supercapacitors.[14-21]

Beyond energy storage, they have also other promising applications such as water purification, lubrication, sensing, catalysis and composite reinforcement.[22-24]

Lithium-ion batteries are well known for a variety of excellent characteristics. High energy density, high power density, long life and environmental friendliness are the main features of LIBs.[25] However, finding a more durable and suitable anode material in LIBs is one of the main challenges for further development of these batteries.[26,27] Although MXenes have high volumetric capacities as electrode material, presence of functional groups or defects on their surface might lead to the irreversible lithium storage and efficiency decrease of LIBs.[18] On the other hand, titanium dioxide (TiO_2) is an interesting material for photocatalysis, purification and energy generation and storage applications,[28-34] due to its thermal and chemical stability, mechanical hardness and non-toxicity.[35-37] Nevertheless, application of pure TiO_2 for energy storage applications such as LIBs is limited because of its relatively moderate storage capacity and low conductivity.[38] Moreover, electrochemical properties of TiO_2 depend on the particle size.[39,40] Thus, designing new TiO_2-based systems in order to overcome those limitations is very essential, especially for LIB applications.

It has been found that combining TiO_2 with carbon materials is a beneficial method to improve the properties of TiO_2 through promoting the electron transport from carbon and increasing the accessible surface area of TiO_2.[41] Titania-carbon hybrids have superior performance in LIBs and photocatalysts. Most common methods of synthesis of TiO_2 supported carbonaceous materials are two-step techniques including chemical vapor deposition and sol–gel processes.[42,43] Recently, oxidation of MXene structures has been proposed as an alternative one-step synthesis method, which can provide the well-controlled formation of TiO_2 on carbon substrate.[38,44-46] Naguib *et al.* experimentally showed that heating Ti_3C_2 MXene in air leads to the growth of TiO_2 nanocrystals

on disordered graphitic carbon structures.[44] They reported that the resulting titania-carbon hybrids reveals extremely high cycling rates as anodes in LIBs. It was shown that oxidation of MXene in CO_2 and pressurized water also leads to the formation of titania-carbon hybrids. In another experimental work, layered titania was synthesized by a hydrothermal reaction of MXene followed by oxidation in air.[45] The layered TiO_2 structure exhibited good electrochemical properties in LIBs. Moreover, Ahmed *et al.* demonstrated that treatment of MXene with H_2O_2 leads to opening up of MXene sheets and formation of TiO_2 nanocrystals on their surface.[46] H_2O_2 treated MXene, as anode material, significantly enhanced the performance of LIBs in comparison to the as-prepared MXenes.

Despite the progress in the experimental synthesis of different anode materials for LIBs such as titania-carbon hybrids, the cost, complexity and time-consuming nature of these processes motivates the researchers to develop computational tools for getting deeper insight on the atomic structures and designing more efficient materials. Reactive molecular dynamics simulations provide crucial information on the atomistic details of different materials as well as realistic representation of chemical interactions. ReaxFF is a reactive force field which has the capability of simulating chemical reactions with accurate transition states.[47-50] The level of accuracy of ReaxFF is comparable to quantum calculations, with the advantage of simulating bigger systems and longer time scales. ReaxFF methods have been extensively used for a wide range of applications such as energy storage materials.[51-53] ReaxFF was also successfully used for simulating a number of water/surface interfaces.[54-56] Moreover, modeling the interaction of water with different orientations of TiO_2 surfaces was implemented by using ReaxFF simulations.[57] Recently, the interaction of $Ti_3C_2T_x$ MXene layers with intercalated pure water and metal ions was investigated by ReaxFF description.[58] To the best of our knowledge, there is no published

work on the oxidation of MXene structures by using molecular dynamics simulations. Thus, modeling MXene oxidation by ReaxFF molecular dynamics simulations will be very effective and useful.

The main aim of this paper is to investigate the oxidation of MXene structures in three different environments including dry air, wet air and hydrogen peroxide by using ReaxFF based molecular dynamics simulations. The organization of this paper is as follows. First, an introduction to the computational model will be presented. After that, the simulation setup and experimental sections are discussed. Next, MXene oxidation with oxygen, water/oxygen and H_2O_2 molecules will be presented. Finally, MXene heating in vacuum will be presented and its comparison with other environments will be discussed.

2. Methods

2.1. Computational Method

ReaxFF is a bond-order-based reactive force field technique which can consider bond formation and bond dissociation during molecular dynamics simulation. Bond orders are directly calculated between all pairs of atoms from the interatomic distances at every iteration. Accordingly, smooth transition between the non-bonded states and single, double or triple bonded states would be possible, leading to the simulation of chemical reactions and transition states properly. The total energy in ReaxFF is described by the following energy terms:

$$E_{system} = E_{bond} + E_{under} + E_{over} + E_{val} + E_{tor} + E_{lp} + E_{vdw} + E_{coulombic} \quad (1)$$

The energy of the system (E_{system}) includes bonded or covalent interactions (bond order dependent) and non-bonded interactions. Bond order dependent terms include bond energy (E_{bond}), under coordination (E_{under}) and over-coordination (E_{over}). Valance-angle energy (E_{val}),

torsion-angle energy (E_{tor}) and lone pair energy (E_{lp}) are energy penalty terms. Non-bonded interactions include van der Waals (E_{vdw}) and Coloumb energy ($E_{coulomb}$) and are taken into account between each pair of atoms in the system. Atomic charges are derived from an electronegativity equalization method (EEM)[59] with a shielding term to prevent excessive short-range interactions. Here, we used parameters of Ref 58 for ReaxFF force field.

2.2. Simulation Setup

In order to investigate the effect of dry air, wet air and H_2O_2 molecules on the oxidation of MXene structures, we performed a series of MD-NVT simulations on MXene in the presence of 200 oxygen molecules (dry air environment), 100 oxygen and 100 water molecules (wet air environment) and 200 hydrogen peroxide molecules (H_2O_2 environment). Note that we didn't consider nitrogen atoms in the air, due to their neutral effects in the simulations. We used an oxygen terminated MXene structure ($Ti_3C_2O_2$). Simulations were performed at temperatures of 1000, 1500, 2000, 2500 and 3000 K for 1,000,000 MD-time steps (100 picoseconds). Please note that because of time-scale limitation of molecular dynamics simulations, which needs femtosecond time steps to resolve individual bond vibrations, we need to choose higher temperatures than experiment to accelerate the dynamics of the system during a short time scale of MD simulation. The time step in the present work was selected as 0.1 fs. The temperature was controlled by Berendsen thermostat[60] with damping constant of 50 fs.

2.3 Experimental Section

MXene synthesis: $Ti_3C_2T_x$ MXene was synthesized by etching Al from Ti_3AlC_2 using a mixture of aqueous hydrochloric acid (HCl) and lithium fluoride (LiF) similar to what was reported by

Ghidiu et al..[61] In short, 10 g of -400 mesh powder of Ti_3AlC_2 (more details about the synthesis of Ti_3AlC_2 can be found in Ref 9 was slowly added to a solution of 6.6 g of LiF (99.98%, Alfa Aesar) dissolved in 100 mL of 6 M aqueous HCl (37%, Sigma-Aldrich). Then, the mixture was heated to 40 °C and continuously stirred for 45 h at that temperature. After etching time elapsed, the sediment was separated from the liquid by centrifuging at 3500 rpm followed by decanting the liquid, and fresh deionized (DI) water was added to wash the sediment. The steps of centrifuging, decanting the liquid, and adding fresh DI water were repeated several times till the pH of the liquid after centrifuging reached values more than 5. The sediment was then dried at room temperature (RT) using a vacuum-assisted filtration device. To produce free-standing $Ti_3C_2T_x$ paper, 0.5 g of the dried powder was added to 50 mL of DI water and sonicated in an ultrasound water bath for 1 h then centrifuged at 3500 rpm for 1 h. The black supernatant was then decanted from the centrifuging tube and filtered through a Celgard membrane (3501 Coated PP, Celgard, USA). Finally, the membrane with filtered material was allowed to dry at RT in air for 18 h, then the MXene paper was detached from the membrane.

Heat treatment experiments: An alumina tube furnace was heated to either 1000 K or 1500 K. Then a piece of the MXene paper placed in an alumina boat was introduced to the furnace's hot zone and held there for 30 s, then pulled out from the furnace and removed from the boat for further characterization. When wet air was used, the tube was open from both ends to use the lab air environment that has relative humidity of about 30%. For dry air condition, an air gas tank of UN1002 (Al UZ300, Ultra Zero Grade Air, Airgas) was connected to one end of the tube and continuous flow of air from the tank was maintained to ensure minimal, if any, backflow of lab air into the furnace from the open end of the tube that was used to introduce the sample during the heat treatment process. Annealing under argon (Ar) was carried out by placing a piece of the

MXene paper in the furnace at RT then the furnace was heated to 1500 K (at heating rate of 600 °C/h) and held at this temperature for 0.5 h then furnace was allowed to cool down freely till it reached RT, with an argon gas continuous flow during the entire process. Note that due to experimental setup limitations, we did not use H_2O_2 as oxidation agent.

Characterization: A Scintag X1 Cu K_α X-ray diffractometer (Scintag, Cupertino, CA, USA) was used to investigate the changes in the structure of the MXene paper before and after heat treatment. In all cases, 45kV and 35 mA were used to power the X-ray tube and a 2 theta step size of 0.02° with dwell time of 1 s at each step were used to collect the X-ray diffraction (XRD) patterns. Raman spectra were collected using a solid state 532 nm excitation laser (Witec Alpha 300 confocal Raman microscope). Laser power was adjusted to be 90 μW in order to prevent laser heating.

3. Results and Discussions

3.1. Oxidation of MXene by Dry Air

To assess the oxidation of MXene structure in dry air, MD-NVT simulations were performed at different temperatures. Fig. 1(a) shows the initial system containing MXene structure with 200 O_2 molecules. The dimension of periodic box is 26.25×30.3×133.66 $Å^3$. Fig. 1(b) represents the evolution of MXene structure by time after 0, 50, 75 and 100 ps of oxidation in the presence of O_2 molecules at 1500K. For clarification, the gas components have been removed and only MXene structure has been represented in these figures. As can be seen, at simulation time of 25 ps, no significant change is observed in the MXene structure, while at time of 50 ps, some Ti atoms at surface of MXene are making bond with oxygen molecules in the environment. At

simulation times of 75 and 100 ps, the structure is completely distorted, since the Ti atoms in the middle layer diffuse to the top and bottom surfaces binding with O_2 molecules in the environment. Consequently, the two separate carbon layers get closer to each other, leading to the formation of C-C bonds. In order to observe this phenomenon more clearly, we have represented the change in the configuration of C atoms in the MXene structure by simulation time in the bottom of Fig. 1b. As shown, after 75 ps, C atoms are making bond to each other, leading to the formation of a carbon substrate.

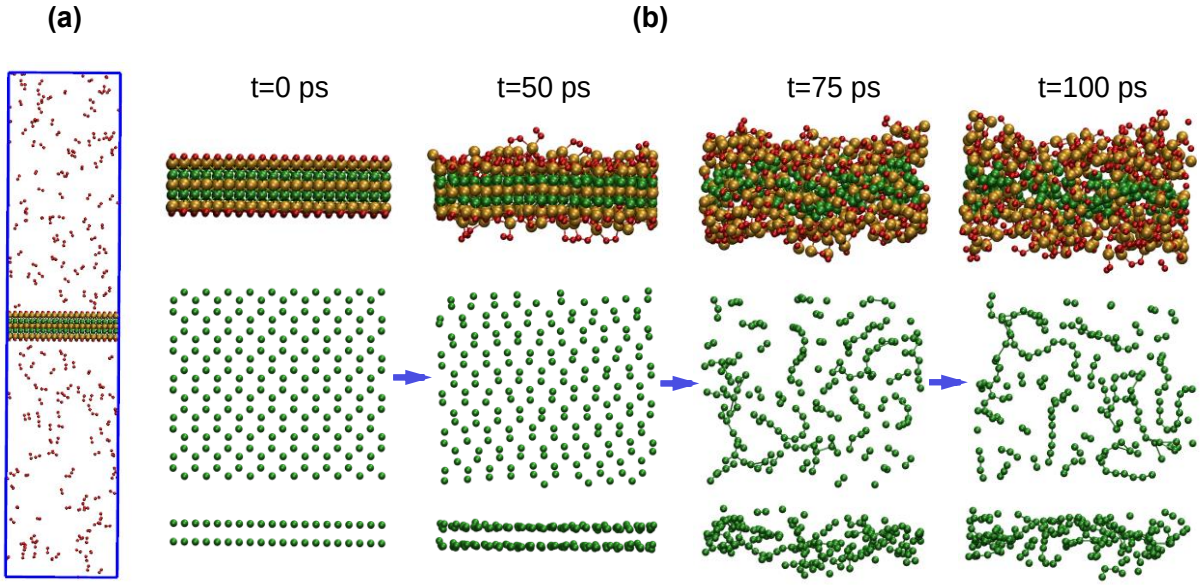

Fig. 1. (a) Initial structure including MXene structure with 200 O_2 molecules, (b) MXene structure and the change in the configuration of C atoms existing in the MXene structure (top and side views) after 0, 50, 75 and 100 ps oxidation in the presence of O_2 molecules at 1500K (Ti: tan, C: green, O: red)

Fig. 2 shows different views of the final structure of the ReaxFF simulation after oxidation of MXene in the presence of O_2 molecules at 1500K. Our results are in agreement with the experiment[44], in which the authors revealed that oxidation of MXene leads to the growth of

laterally shrinked titania nanopaticles over the carbon substrate. They mentioned that shrinkage of these nanoparticles is related to the diffusion of Ti atoms from the middle layer to the MXene flake surfaces. If we look at the top and bottom views of our ReaxFF results, similar shrinkage of TiO_2 nanoparticles is observed.

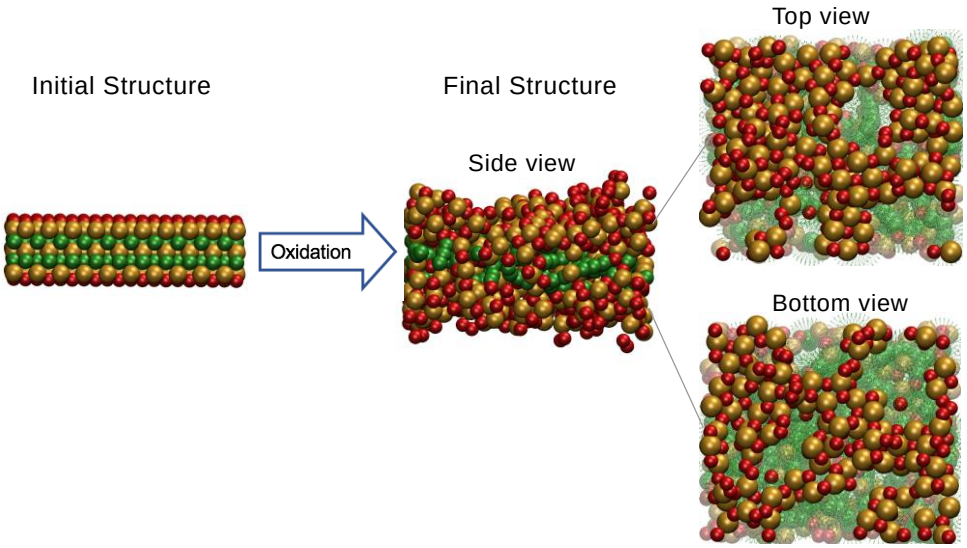

Fig. 2. Growth of laterally shrinked titania nanopaticles over the carbon substrate after oxidation of MXene in the presence of O_2 molecules at 1500K (For top and bottom view, carbon substrate is represented with dotted format) (Ti: tan, C: green, O: red)

To analyze the diffusion pass of Ti atoms in the middle layer to the surface, we used Nudged Elastic Band (NEB) calculation. Fig. 3a shows that during heating MXene at 1500K in the presence of dry air, some defects are created in the MXene surface and are enlarged by time. As a result, some O atoms diffuse to the MXene structure and help the Ti atoms in the middle layer to diffusing to the surface to make TiO_2 structure. Fig. 3b shows the diffusion pass of a Ti atom in the middle layer within defect cite to the top surface. Fig. 3c indicates that the energy barrier for this diffusion is around 2.8 eV, and the final structure is more stable than the initial structure

by 2.3 eV. Although this energy barrier is a fairly significant barrier, it can be crossed at elevated temperatures.

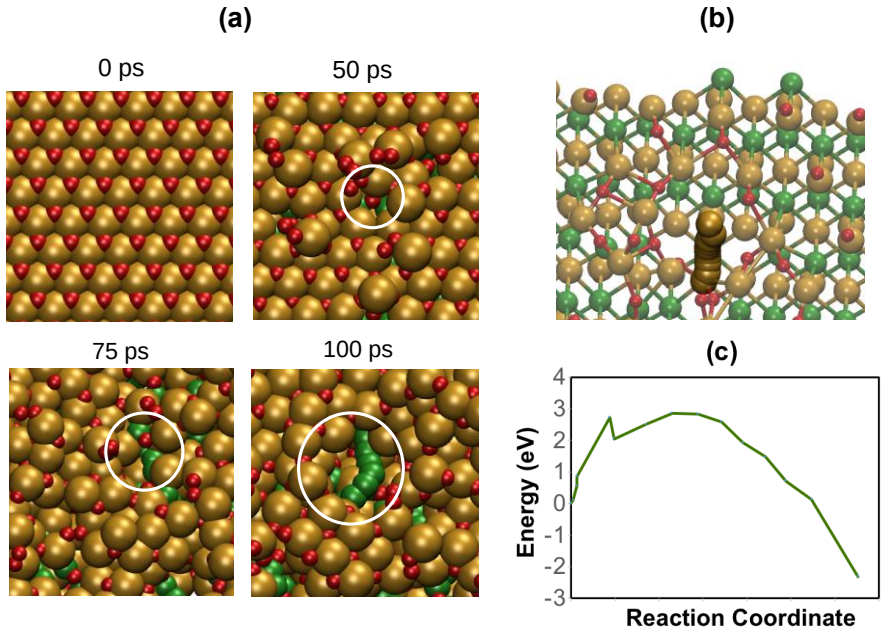

Fig. 3. a) Defect creation and enlargement during MXene heating at 1500K in the presence of dry air, b) diffusion pass of a Ti atom in the middle layer within the defect cite to the top surface, c) energy curve for the diffusion of Ti atom in the middle layer to the top surface. (Ti: tan, C: green, O: red)

In order to have a detailed survey on the bond changes during the oxidation of MXene, we calculated the average bond number for C-C, Ti-C and C-C at different simulation times. Average bond number for A-B was calculated by the division of total number of A-B bonds in the structure to the total number of A atoms in the structure. Fig. 4 shows the change in the average bond number for C-C, Ti-C and Ti-O during the oxidation of MXene structure in dry air at 1500 K. The results indicate that for C-C, the average bond number increases from 0 to 1.54 which is related to the creation of C-C bonds during the NVT simulation of MXene oxidation. For Ti-C, the average bond number decreases from 3.0 to 0.6, indicating that Ti-C bonds are

breaking during the oxidation of MXene at 1500 K. On the other hand, the average bond number of Ti-O increases from 2.0 to 3.46, which is related to the creation of new bonds between Ti and O atoms due to MXene oxidation at 1500 K. These results are in agreement with the experimental X-ray photoelectron spectroscopy (XPS) analysis for MXene oxidation.[46] The authors indicated that during the oxidation of MXene, the intensity of Ti-C peak decreases in XPS spectra, while the intensity of Ti-O peak increases, indicating that TiO_2 nanoparticles are being formed. Note that although these experimental results are related to the oxidation of MXene with H_2O_2, as we will show later, the trend for the change in the bond order during the MXene oxidation with H_2O_2 is similar to the dry air.

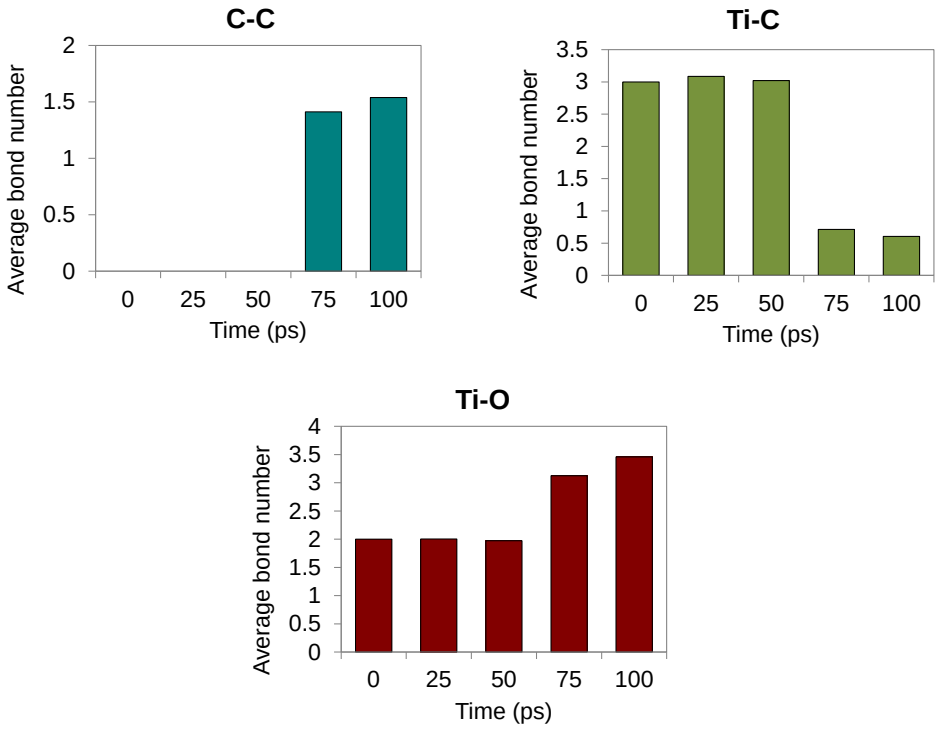

Fig. 4. Change in the average bond number for C-C, Ti-C and C-C during the oxidation of MXene structure with dry air at 1500 K

To investigate the effect of temperature in the oxidation of MXene with dry air, in addition to 1500K, we also performed NVT simulations at different temperatures of 1000K, 2000 K, 2500 K and 3000K. Fig. 5 represents the final MXene structure after oxidation at these temperatures. As it can be seen, at 1000 K, neither surface functionalization nor TiO_2 nanoparticle formation is observed. At 1500 K and 2000 K, C atoms are bonding to each other to create a substrate. At higher temperatures, surface opening occurs at the top and bottom layers and by time increase, the defects are enlarged and consequently, C atoms migrate to the surface of MXene structure. For instance, at temperature of 2500 K, carbon chains diffuse to the surface and at temperature of 3000 K, some carbon chains are released to the gas phase.

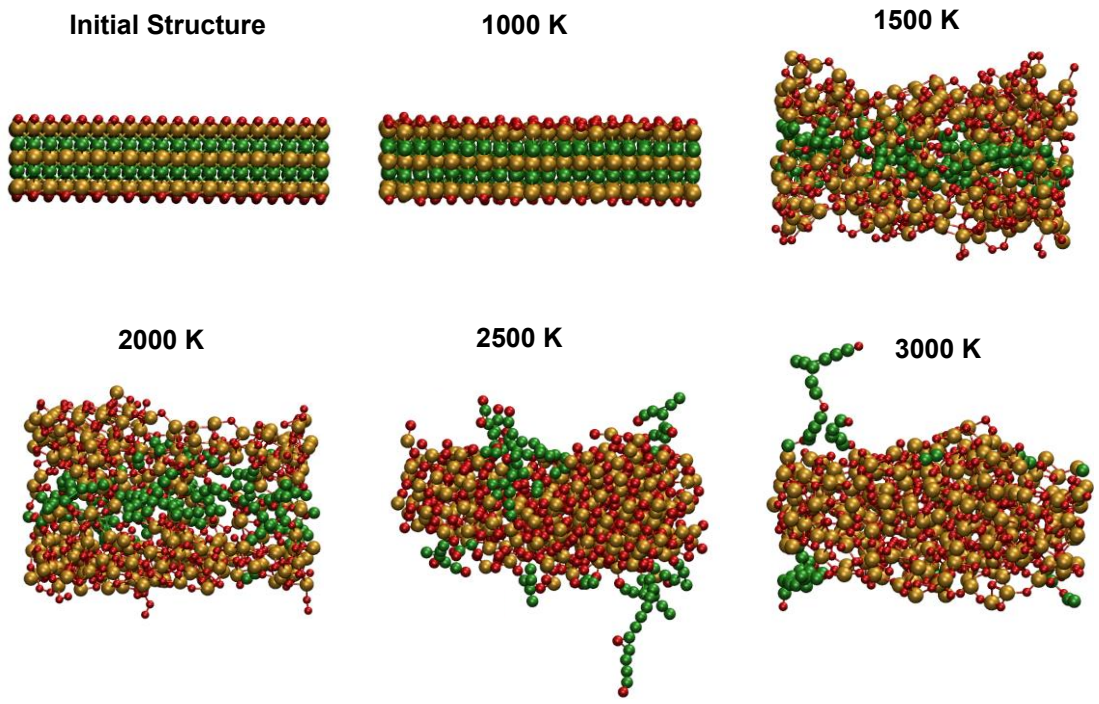

Fig. 5. Final MXene structure after oxidation in dry air at temperatures of 1000 to 3000 K (Ti: tan, C: green, O: red)

To check the bond characteristics of the MXene structure during the oxidation with dry air, we calculated the radial distribution functions (RDFs). Fig. 6a represents the RDF results for C-C at different temperatures. In the initial MXene structure, C atoms are organized as a crystalline structure with a far distance of 3 Å from each other, revealing that no C-C bond exist in the initial MXene structure. RDF of C-C in MXene structure at 1000 K is similar to the initial structure, which reconfirms that there is no significant change in the MXene structure due to oxidation with dry air at 1000 K. At temperature of 1500 K, the structure becomes amorphous with the appearance of first and second peaks at about 1.2 and 1.5 Å, revealing that C-C bonds have been formed. By temperature increase the intensity of peaks at distance of 1-2 Å increases. Thus, RDF analysis also confirms our previous results, that due to oxidation of MXene structure at higher temperatures, C-C bonds are being created in the MXene structure.

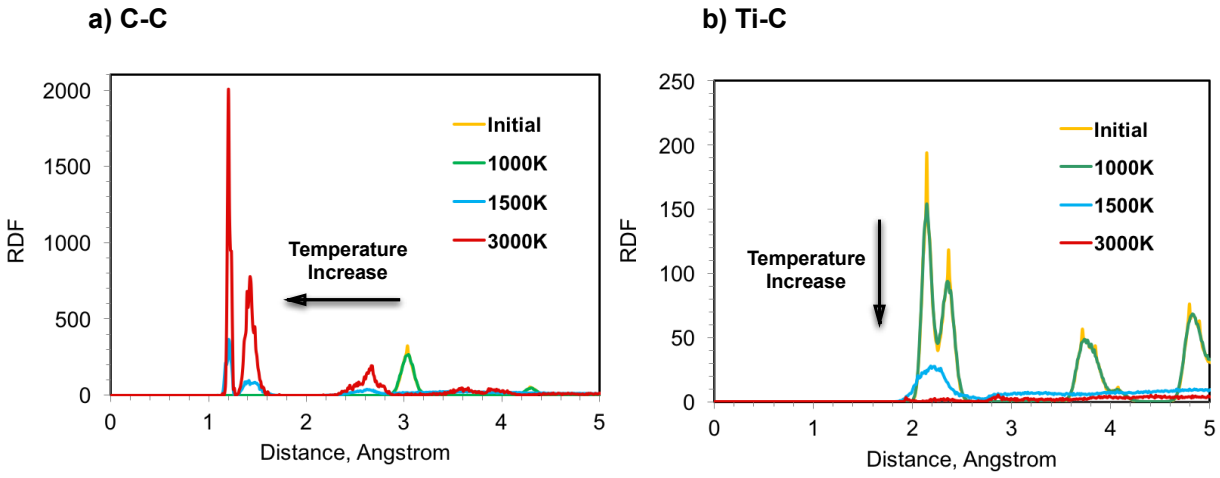

Fig. 6. RDF results for a) C-C, b) Ti-C in MXene structure after oxidation in dry air at different temperatures

Fig. 6b shows the RDF results for Ti-C at different temperatures. In initial MXene structure, Ti-C bonds are organized as a crystalline structure with a distance of 2.1 and 2.4 Å. RDF of Ti-C in

MXene structure at 1000 K is similar to the initial structure. Due to oxidation of MXene at 1500 K, the structure becomes amorphous with a broad peak at 2.2 Å. The intensity of this peak is much lower than the initial structure, indicating that many Ti-C bonds have been broken. By temperature increase, the intensity of peaks at distance of 2-3 Å disappear, revealing that almost all Ti-C bonds have been broken. RDF results for Ti-C also confirms our previous results, that by oxidation of MXene structure at high temperatures, Ti-C bonds are being broken.

3.2. Comparison of Mxene Oxidation in Different Environments

We repeated the above-mentioned simulations for oxidation of MXene structure in the presence of wet air (O_2 and H_2O molecules) as well as in the presence of H_2O_2 molecules. The trends for oxidation of MXene were similar to the case of dry air. However, there is a significant difference in the rate of degradation for these materials. Fig. 7 shows the comparison between these three environments. For example, at 100 ps and at temperature of 1000K, in case of oxidation with dry air, there is no change in the MXene structure, while in case of oxidation with wet air some Ti atoms migrate to the surface of MXene structure and the surface is functionalized with O and OH functional groups. For case of oxidation with H_2O_2, the oxidation rate is much higher than dry and wet air and many functional groups are observed on the surface of MXene structure. Similar result is observed at 25 ps and temperature of 1500 K. Therefore, it can be concluded that the order for oxidation rate of MXene structure in different environments is as following: H_2O_2 > Wet Air > Dry Air.

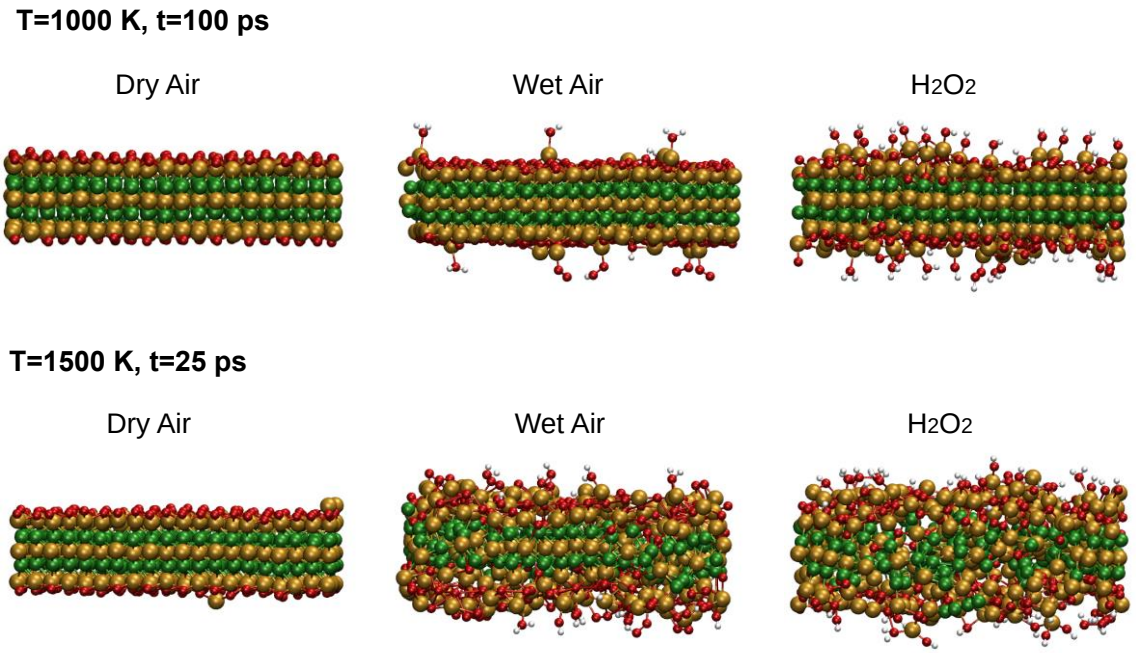

Fig. 7. The comparison among oxidation rates of MXene at three different environments (Ti: tan, C: green, O: red, H: white)

3.3. Analysis of Gas Phase Components during MXene Oxidation in Different Environments

For further analysis of reactions occurring during the oxidation, we analyzed the gas phase components. Fig. 8 represents the comparison among the gas phase components of MXene oxidation in three different environments at temperatures of 1000, 1500 and 3000K. For case of oxidation in dry air at 1000K, all 200 O_2 molecules are intact at the end of simulation. At 1500 K, 84 O_2 molecules remain intact, and 6 CO and 3 CO_2 are produced, indicating that by temperature increase the rate of oxidization increases. Formation of CO and CO_2 during the oxidation of MXene is consistent with the experiment.[46] Due to diffusion of Ti atoms to the surface and formation of TiO_2 nanoparticles on the surface of MXene, some defects are created on the surface of MXene structures, which provides the opportunity for the diffused O atoms to

be bonded with C atoms, leading to the formation of CO and CO_2. At 3000 K, 15 O_2 molecules remain intact, and 59 CO and 20 CO_2 are produced. In addition to CO and CO_2, some other oxides of carbon such as C_2O_2 are also formed.

For the case of MXene oxidation with wet air, at temperature of 1000 K, 96 O_2 and 94 H_2O remain intact at the end of simulation and no other gas component is created. This result confirms that rate of MXene oxidation in wet air is higher than dry air. The four O_2 and six H_2O molecules are consumed to functionalize the surface of MXene structure, as represented in Fig. 8. At temperature of 1500 K, 16 O_2 and 74 H_2O remain intact at the end of simulation and 10 CO, 2 CO_2 and 1 H_2O_2 molecules are formed. At temperature of 3000 K, 1 O_2 and 75 H_2O molecules remain intact and 13 CO and 2 CO_2 are produced.

For the case of oxidation of MXene with H_2O_2, at temperature of 1000 K, 149 H_2O_2 molecules remain intact at the end of simulation and no other gas component is observed. Note that the high rate of consumption of H_2O_2 molecules at 1000 K, in comparison to dry and wet air, indicates that H_2O_2 is a much stronger oxidant for the oxidation of MXene. Some H_2O_2 molecules are used to functionalize the surface of MXene structure, as represented in Fig. 8. Furthermore, during the heating process at 1000 K, some H_2O_2 molecules are dissociated to make other components such as 7 O_2 and 27 H_2O. At temperature of 1500 K, 51 H_2O_2 molecules remain intact at the end of simulation. In addition, 13 CO, 2 CO_2, 102 H_2O, 2 OH and 4 O_2 are formed. At temperature of 3000 K, no H_2O_2 molecule remains intact and 17 CO, 2 CO_2 and 165 H_2O molecules are produced. Moreover, some other components such as C_2H_2O, $C_2H_2O_2$, OH and H_2 are formed. All these results reconfirm that by temperature increase, the rate of MXene oxidation enhances and the order of oxidation rate in different environments is: H_2O_2 > Wet Air > Dry Air.

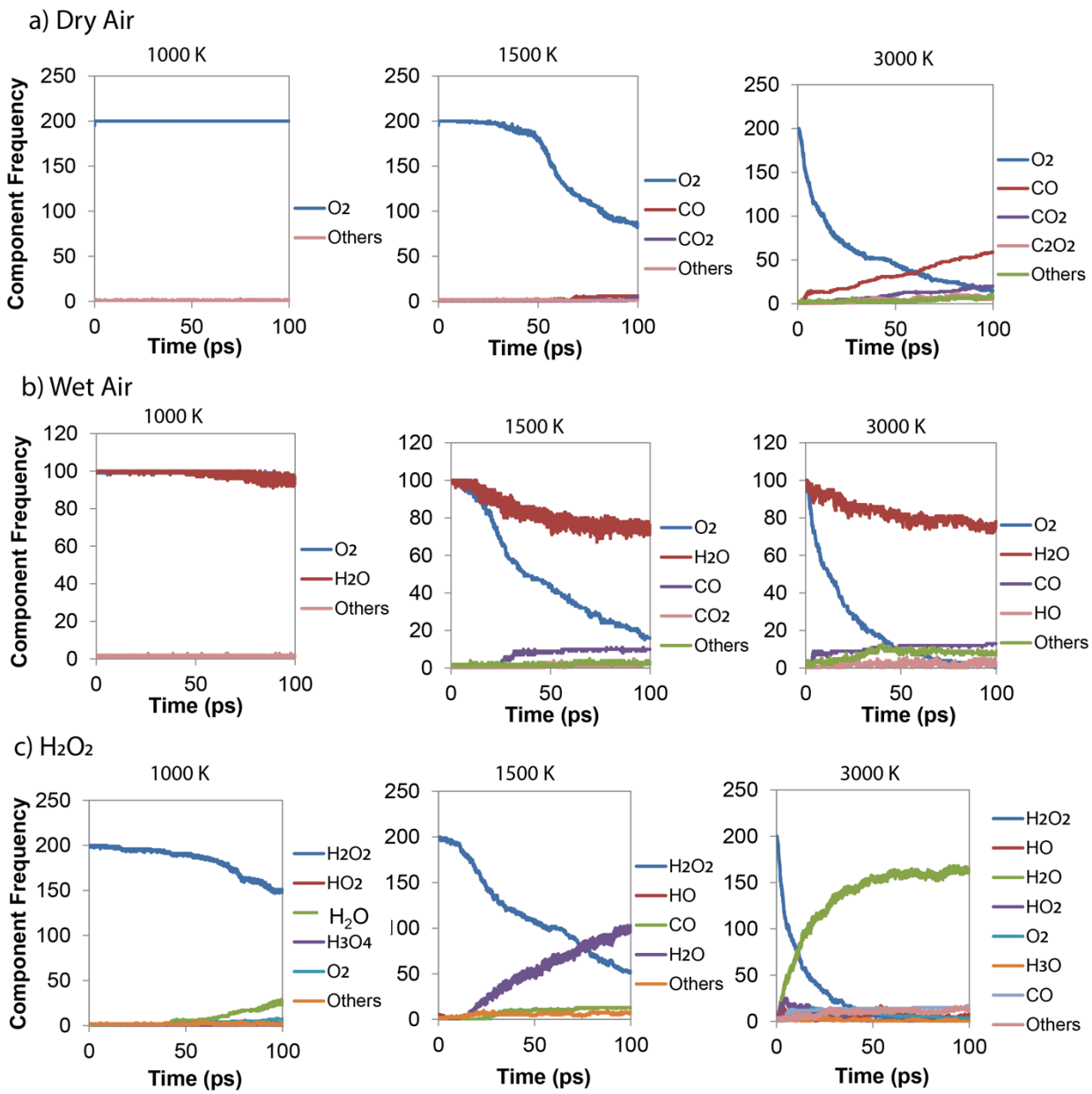

Fig. 8. The comparison among the gas phase components of MXene oxidation in three different environments (dry air, wet air and H_2O_2) at temperatures of 1000, 1500 and 3000K

3.4. Experimental results for MXene Oxidation in Dry and Wet Air

Fig. 9a shows the XRD patterns of $Ti_3C_2T_x$ paper before and after various heat treatments under dry and wet air environments. Heating to 1000 K resulted in broadening of the 002 peak, due to

evolving of another peak at slightly higher 2theta angle (lower *d*-spacing). This can be explained by partial removing of the pillaring water[62] from in-between the MXene layers.[63] The persistence of diffraction peaks at low angles is surprising considering that the samples were heated to 1000 K which in principle should be sufficient for evaporating any intercalated water, but kinetics can be the reason for this considering that the sample was heated for 30 s only. Also, the pillared water may contribute toward the oxidation of MXene, but since the amount of water of the pillars in MXene is very small (atomic ratio of Ti : H_2O ~ 10 : 1)[62] its contribution is minimal. No strong titanium oxide peaks were observed in the XRD patterns after the treatments at 1000 K.

For the 1500 K treatments, a complete loss of the pillaring water resulted in an upshift of the 002 peak to higher angels (2theta of ~8.6° instead of 6.4°) and lowering its intensity. In addition, two new sharp peaks at 2theta of ~25.3° and 27.5° emerged after the treatment, and they can be assigned to anatase(PDF# 21-1272) and rutile(PDF 21-1276), respectively. The ratio of the area under the anatase and rutile peaks (at 2theta of ~ 25.3° and 27.5°, respectively) to the area under the 004 peak of MXene (at 2theta of ~17.4°) was found to be ~1.1 for dry air, and 1.5 for wet air which suggests the presence of more oxide in the sample when MXene was heated in wet air. This result validates our MD simulation that oxidation rate of MXene in wet air is higher than dry air. Although continuous flow of dry air was maintained during the dry air heat treatment processes, the possibility of lab air back flow to the tube furnace and mixing with the flowing dry air cannot be completely ruled out. Thus, differences observed here between wet and dry air heat treated samples can be more pronounced if the dry air experiment is conducted in a dry-room. It is worth noting that the intensity of the anatase peak was stronger than that of rutile for the dry air treatment and the opposite was true in case of wet air treatment. Raman spectra (Fig. 9b)

show two broad bands around 1360 and 1590 cm^{-1} which can be assigned respectively, to the D and G bands of graphitic carbon. The presence of strong and broad disorder-induced band (D band) is an evidence for disordered graphitic carbon[64,65], which is consistent with our simulations.

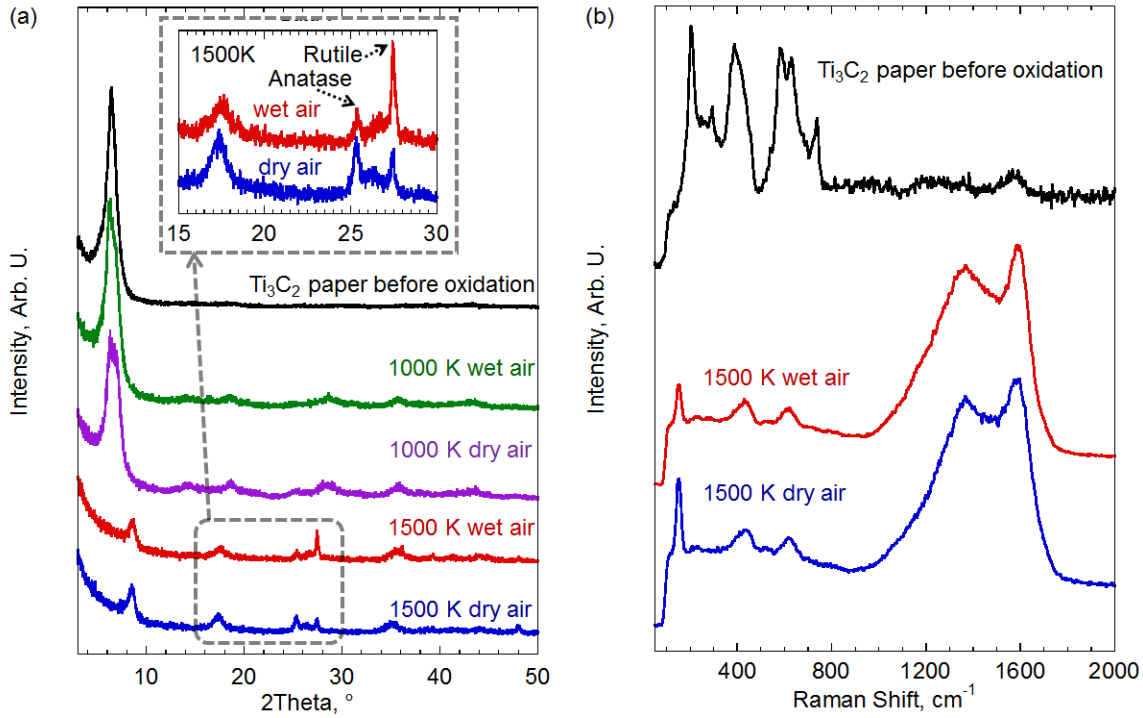

Fig. 9. (a) XRD for Ti_3C_2 paper before (black pattern) and after heat treatments at 1000 K in wet (green pattern) and dry (purple pattern) air, and at 1500 K in wet (red pattern) dry (blue pattern) air 30 s each. The inset is a zoom in on the last two patterns. (b) Raman spectra of Ti_3C_2 paper before (black spectrum) and after heat treatment at 1500 K for 30 s in wet (red spectrum) and dry (blue spectrum) air.

3.4. Heating MXene Structure in Vacuum

To compare the oxidation of MXene in different environments with the case of vacuum, we repeated the NVT simulation for the case of heating MXene in vacuum. The results revealed that due to heating MXene in vacuum, no significant change occurs on MXene structure in terms of formation of C substrate or TiO_2 structure. The reason for this fact is attributed to the lack of

oxidation agent in the environment. However, RDF results from MD simulations indicated that during MXene heating in vacuum at 1500 K, Ti and C atoms are rearranged to form cubic titanium carbide (TiC) structure (Fig. 10a). Our experimental tests also indicated that heating MXene paper at 1500 K under argon resulted in the disappearance of the 002 peak of MXene, and appearance of two new peaks at 2 theta of ~36.2° and 76.8° (Fig. 10b). These peaks can be assigned to highly oriented titanium carbide (PDF# 32-1383) along its 111 plane, which is in agreement with our MD simulations. This high preferred orientation can be explained by the topotactic transformation of layered hexagonal carbide along 00*l* plan to its cubic carbide 111 plan.[66,67] It is worth noting that based on the position of 111 and 222 peaks, the lattice parameter of the formed titanium carbide was found to be ~ 4.29Å, slightly smaller than that of TiC (PDF# 32-1383), which is 4.33Å. The smaller lattice parameter can be explained by deviation from the stoichiometry (Ti:C = 1:1)[68], since the starting Ti:C ratio is 3:2, and oxygen incorporation into structure and formation of oxycarbide is possible.[69]

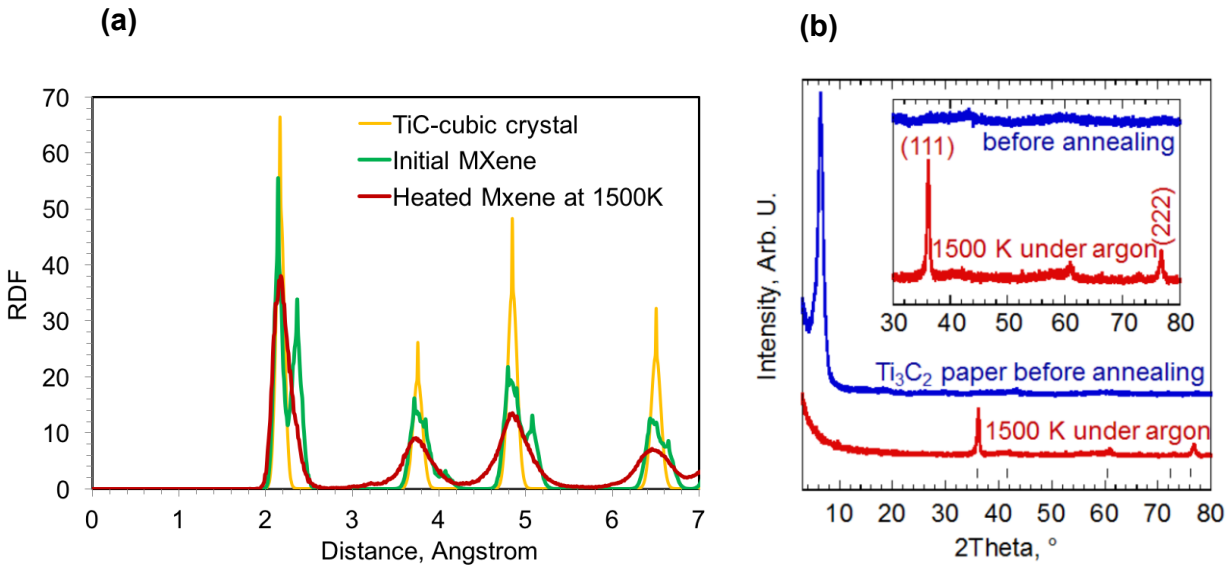

Fig. 10. a) RDF results for Ti-C in cubic TiC crystal, initial MXene structure and after heating at 1500K, b) XRD patterns for Ti_3C_2 paper before (blue pattern) and after annealing at 1500 K under argon for 0.5 h

(red pattern). The vertical black markers represent the peaks position of TiC [PDF# 32-1383]. The inset shows the 2 theta range from 30° to 80°.

Fig. 11 represents the change in the average bond number for C-C, Ti-C and C-C during heating of MXene structure in dry air, wet air, H_2O_2 and vacuum at 1500 K. As shown, for the case of vacuum, average bond orders of C-C, Ti-C and Ti-O do not change significantly, while other environments experience significant change. Thus, presence of oxidation agent, significantly affects the change of bond order in MXene structure.

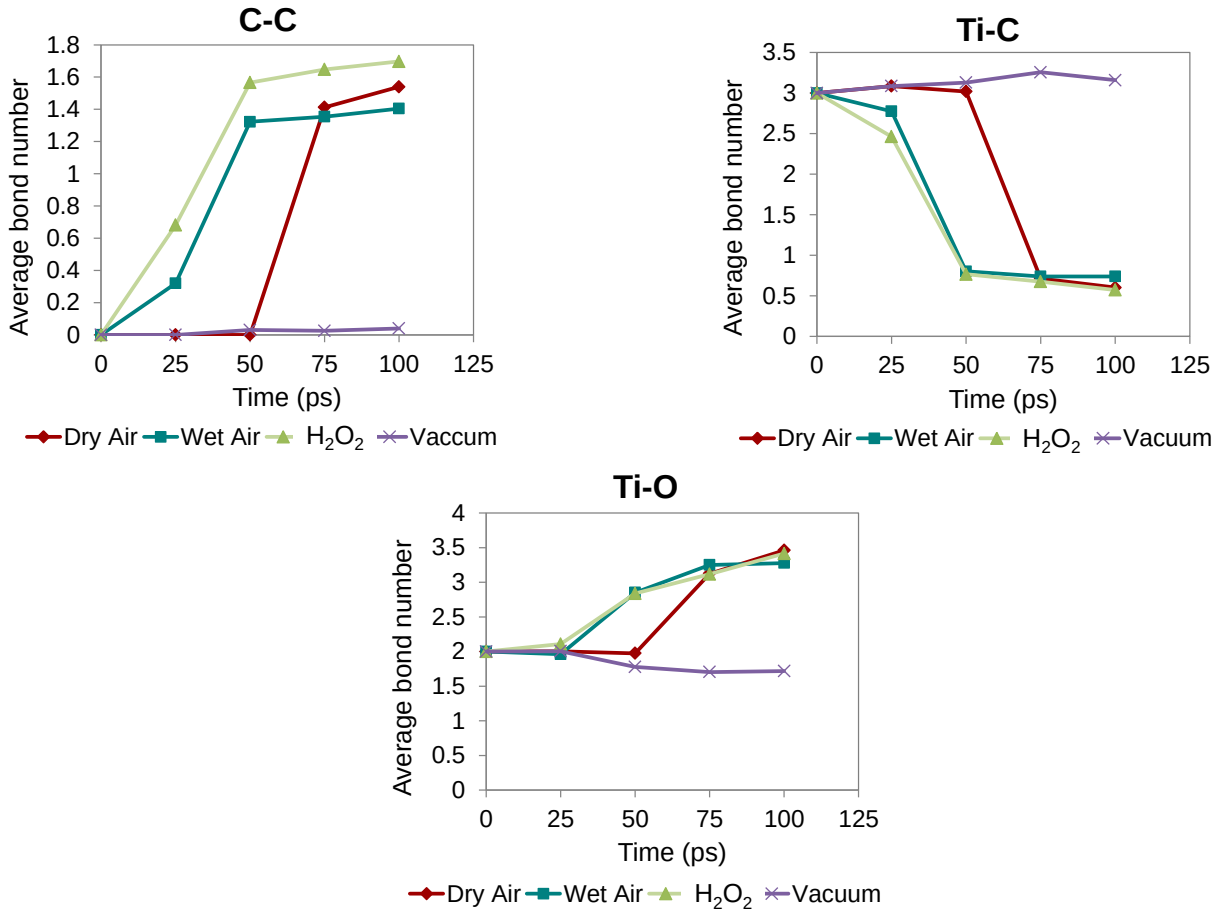

Fig. 11. Change in the average bond number for C-C, Ti-C and C-C during heating MXene structure in dry air, wet air, H_2O_2 and vacuum at 1500 K

4. Conclusions

Carbon supported TiO_2 hybrids has attracted increasing attention due to its unique properties and applications, especially in LIBs. Oxidation of MXene structures has been introduced as a prominent method for the synthesis of these hybrid materials. In the present work, we simulated the oxidation of Ti_3C_2 MXene structures by using ReaxFF at different environments including dry air, wet air and hydrogen peroxide at different temperatures of 1000 K to 3000 K. The results indicated that by temperature control, formation of carbon-TiO_2 hybrid structure would be possible. Furthermore, it was revealed that among different environments, H_2O_2 environment has the strongest rate of MXene oxidation, while dry air has the weakest rate of MXene oxidation. Moreover, heating MXene in vacuum was predicted to result in recrystallization into cubic TiC. The simulation results were validated experimentally by heat treating MXene in dry and wet air in addition to inert gas. The results discussed in this study provides fundamental insights on the chemical stability of MXenes and their plausible chemical transformation under oxidative conditions that could have significant implications in areas such as electrochemical storage, catalysis and sensors.

Conflicts of interest

There are no conflicts to declare.

Acknowledgements

We acknowledge funding from the Fluid Interface Reactions, Structures and Transport (FIRST) Center, an Energy Frontier Research Center funded by the U.S. Department of Energy (DOE), Office of Science, Basic Energy Sciences.

References

1. S.Z. Butler, S.M. Hollen, L. Cao, Y. Cui, J.A. Gupta, H.R. Gutiérrez, T.F. Heinz, S.S. Hong, J. Huang, A.F. Ismach, E. Johnston-Halperin, M. Kuno, V. V. Plashnitsa, R. D. Robinson, R. S. Ruoff, S. Salahuddin, J. Shan, L. Shi, M.G. Spencer, M. Terrones, W. Windl, J. E. Goldberger, *ACS Nano*, 2013, **7**, 2898–2926.

2. V. Nicolosi, M. Chhowalla, M. G. Kanatzidis, M. S. Strano, J. N. Coleman, *Science*, 2013, **340**, 1226419.

3 D. Akinwande, N. Petrone, J. Hone, *Nat. Commun.*, 2014, 5, 5678.

4 G. Fiori F. Bonaccorso, G. Iannaccone, T. Palacios, D. Neumaier, A. Seabaugh, S.K. Banerjee, L. Colombo, *Nat. Nanotechnol.*, 2014, **9**, 768–779.

5 F. H. L. Koppens, T. Mueller, P. Avouris, A. C. Ferrari, M. S. Vitiello, M. Polini, *Nat. Nanotechnol.*, 2014, 9, 780–793.

6 M. Nasilowski, B. Mahler, E. Lhuillier, S. Ithurria, B. Dubertret, *Chem. Rev.*, 2016, **116**, 10934–10982.

7 F. Xia, H. Wang, D. Xiao, M. Dubey, A. Ramasubramaniam, *Nat. Photonics*, 2014, **8**, 899–907.

8 M. W.Barsoum, *Progress in Solid State Chemistry*, 2000, **28**, 201-281.

9 M. Naguib, V. N. Mochalin, M. W. Barsoum, Y. Gogotsi, *Adv. Mater.*, 2014, **26**, 992–1005.

10 M. Naguib M. Kurtoglu, V. Presser, J. Lu, J. Niu, M. Heon, L. Hultman, Y.Gogotsi, M. W. Barsoum, *Adv. Mater.*, 2011, **23**, 4248–4253.

11 M. Naguib, O. Mashtalir, J. Carle, V. Presser, J. Lu, L. Hultman, Y. Gogotsi, M. W. Barsoum *ACS Nano*, 2012, **6**, 1322–1331.

12 M. Naguib, Y. Gogotsi, *Acc. Chem. Res.*, 2014, **48**, 128–135.

13 B. Anasori, M. R. Lukatskaya, Y. Gogotsi, *Nat. Rev. Mater.*, 2017, **2**, 16098.

14 M. R. Lukatskaya, O. Mashtalir, C.E. Ren, Y. Dall'Agnese, P. Rozier, P.L. Taberna, M. Naguib, P. Simon, M.W. Barsoum, Y. Gogotsi, *Science*, 2013, **341**, 1502–1505.

15 Y. Dall'Agnese, M. R. Lukatskaya, K. M. Cook, P. L. Taberna, Y. Gogotsi, P. Simon, *Electrochem. Commun.*, 2014, **48**, 118–122.

16 J. Come M. Naguib, P. Rozier, M.W. Barsoum, Y. Gogotsi, P.L. Taberna, M. Morcrette, P. Simon, *J. Electrochem. Soc.*, 2012, **159**, 1368–1373.

17 M. Q. Zhao, C.E. Ren, Z. Ling, M.R. Lukatskaya, C. Zhang, K.L. Van Aken, M.W. Barsoum, Y. Gogotsi, *Adv. Mater.*, 2015, **27**, 339–345.

18 M. Naguib, J. Come, B. Dyatkin, V. Presser, P.L. Taberna, P. Simon, M.W. Barsoum, Y. Gogotsi, *Electrochem. Commun.*, 2012, **16**, 61–64.

19 M. Naguib, J. Halim, J. Lu, K.M. Cook, L. Hultman, Y. Gogotsi, M.W. Barsoum, *J. Am. Chem. Soc.*, 2013, **135**, 15966–15969.

20 O. Mashtalir, M. R. Lukatskaya, M. Q. Zhao, M. W. Barsoum, Y. Gogotsi, *Adv. Mater.*, 2015, **27**, 3501–3506.

21 X. Liang, A. Garsuch, L. F. Nazar, *Angew. Chem. Int. Ed.*, 2015, **54**, 3907–3911.

22 F. Wang, C. Yang, M. Duan, Y. Tang, J. Zhu, *Biosens. Bioelectron.*, 2015, **74**, 1022–1028.

23 Z. Ling, C.E. Ren, M.Q. Zhao, J. Yang, J.M. Giammarco, J. Qiu, M.W. Barsoum, Y. Gogotsi, *Proc. Natl. Acad. Sci.*, 2014, **111**, 16676–16681.

24 Y. Ying, Y. Liu, X. Wang, Y. Mao, W. Cao, P. Hu, X. Peng, *ACS Appl. Mater. Interfaces*, 2015, **7**, 1795–1803.

25 L. Lu, X. Han, J. Li, J. Hua, M. Ouyang, *J. Power Sources*, 2013, **226**, 272–288.

26 J.M. Tarascon, M. Armand, *Nature*, 2001, **414**, 359–367.

27 V. Etacheri, R. Marom, R. Elazari, G. Salitra, D. Aurbach, *Energy Environ. Sci.*, 2011, **4**, 3243–3262.

28 S. Yadav, G. Jaiswar, *J. Chin. Chem. Soc.*, 2017, **64**, 103-116.

29 A. Fujishima, *nature*, 1972, **238**, 37–38.

30 H. Zhang, G. Chen, D. W. Bahnemann, *J. Mater. Chem.*, 2009, **19**, 5089–5121.

31 Z. Lai, F. Peng, H. Wang, H. Yu, S. Zhang, H. Zhao, *J. Mater. Chem. A*, 2013, **1**, 4182–4185.

32 M. Grätzel, *Nature*, 2001, **414**, 338–344.

33 J. S. Chen, H. Liu, S. Z. Qiao, X. W. D. Lou, *J. Mater. Chem.*, 2011, **21**, 5687–5692.

34 Z. Hong, M. Wei, *J. Mater. Chem. A*, 2013, **1**, 4403–4414.

35 M. Anpo, M. Takeuchi, *J. Catal.*, 2003, **216,** 505–516.

36 U. Diebold, *Surf. Sci. Rep.*, 2003, **48**, 53–229.

37 M. Ni, M. K. Leung, D. Y. Leung, K. Sumathy, *Renew. Sustain. Energy Rev.*, 2007, **11**, 401–425.

38 H. Ghassemi W. Harlow, O. Mashtalir, M. Beidaghi, M.R. Lukatskaya, Y. Gogotsi, M.L.Taheri, *J. Mater. Chem. A*, 2014, **2**, 14339–14343.

39 M. Wagemaker, W. J. Borghols, F. M. Mulder, *J. Am. Chem. Soc.*, 2007, **129**, 4323–4327.

40 C. Jiang, M. Wei, Z. Qi, T. Kudo, I. Honma, H. Zhou, *J. Power Sources*, 2007, **166**, 239–243.

41 R. Leary, A. Westwood, *Carbon*, 2011, **49**, 741–772.

42 G. L. Puma, A. Bono, D. Krishnaiah, J. G. Collin, *J. Hazard. Mater.*, 2008, **157**, 209–219.

43 U. G. Akpan, B. H. Hameed, *Appl. Catal. Gen.*, 2010, **375**, 1–11.

44 M. Naguib, O. Mashtalir, M.R. Lukatskaya, B. Dyatkin, C. Zhang, V. Presser, Y. Gogotsi, M.W. Barsoum, *Chem. Commun.*, 2014, **50**, 7420–7423.

45 H. Tang, S. Zhuang, Z. Bao, C. Lao, Y. Mei, *Chem. Electro. Chem.* , 2016, **3**, 871–876.

46 B. Ahmed, D. H. Anjum, M. N. Hedhili, Y. Gogotsi, H. N. Alshareef, *Nanoscale*, 2016, **8**, 7580–7587.

47 A. C. Van Duin, S. Dasgupta, F. Lorant, and W. A. Goddard, *J. Phys. Chem. A*, 2001, **105**, 9396–9409.

48 K. Chenoweth, A. C. Van Duin, and W. A. Goddard, *J. Phys. Chem. A*, 2008, 112, 1040–1053.

49 T. P. Senftle, S. Hong, M.M. Islam, S.B, Kylasa, Y. Zheng, Y.K. Shin, C. Junkermeier, R. Engel-Herbert, M.J. Janik, H.M. Aktulga, T. Verstraelen, A. Grama, A.C.T. van Duin, *Npj Comput. Mater.*, 2016, **2**, 15011, 2016.

50 M. M. Islam, G. Kolesov, T. Verstraelen, E. Kaxiras, and A. C. van Duin, *J. Chem. Theory Comput.*, 2016, **12**, 3463–3472.

51 M. M. Islam, A. Ostadhossein, O. Borodin, A.T. Yeates, W.W. Tipton, R.G. Hennig, N. Kumar, A.C.T. van Duin, *Phys. Chem. Chem. Phys.*, 2015, **17**, 3383–3393.

52 R. Lotfi, A. S. M. Jonayat, A. C. van Duin, M. M. Biswas, R. Hempstead, *J. Phys. Chem. C*, 2016, **120**, 27443-27451.

53 M. M. Islam, V. S. Bryantsev, A. C. van Duin, *J. Electrochem. Soc.*, 2014, **161**, 3009–3014.

54 J. L. Achtyl, R.R. Unocic, L. Xu, Y. Cai, M. Raju, W. Zhang, R.L. Sacci, I.V. Vlassiouk, P.F. Fulvio, P. Ganesh, D.J.Wesolowski, S. Dai, A. C. T. van Duin, M. Neurock, F. M. Geiger, *Nat. Commun.*, vol. 6, 2015.

55 M. A. Qomi, K.J. Krakowiak, M. Bauchy, K.L. Stewart, R. Shahsavari, D. Jagannathan, D.B. Brommer, A. Baronnet, M.J. Buehler, S. Yip, F.J. Ulm, K.J. Van Vliet, R.J.M. Pellenq, *Nat. Commun.*, 2014, **5**, 4960.

56 M. C. Pitman and A. C. Van Duin, *J. Am. Chem. Soc.*, 2012, **134**, 3042–3053.

57 M. Raju, A. C. Van Duin, K. A. Fichthorn, *Nano Lett.*, 2014, **14**, 1836–1842.

58 N. C. Osti, M. Naguib, A. Ostadhossein, Y. Xie, P.R. Kent, B. Dyatkin, G. Rother, W.T. Heller, A.C.T. van Duin, Y. Gogotsi, E. Mamontov, *ACS Appl. Mater. Interfaces*, 2016, **8**, 8859–8863.

59 W. J. Mortier, S. K. Ghosh, S. Shankar, *J. Am. Chem. Soc.*, 1986, **108**, 4315–4320.

60 H. J. Berendsen, J. van Postma, W. F. van Gunsteren, A. DiNola, J. R. Haak, *J. Chem. Phys.*, 1984, **81**, 3684–3690.

61 M. Ghidiu, M. R. Lukatskaya, M. Q. Zhao, Y. G. Gogotsi, M. W. Barsoum, *Nat. Lond.*, 2014, **516**, 78.

62 E. S. Muckley, M. Naguib, H.W. Wang, L. Vlcek, N.C. Osti, R.L. Sacci, X. Sang, R.R. Unocic, Y. Xie, M. Tyagi, E. Mamontov, K. L. Page, P. R. C. Kent, J. Nanda, I. N. Ivanov, *ACS Nano*, 2017, **11**, 11118-11126.

63 M. Ghidiu, J. Halim, S. Kota, D. Bish, Y. Gogotsi, M. W. Barsourm, *Chem. Mater.*, 2016, **28**, 3507–3514.

64 F. Tuinstra, J. L. Koenig, *J. Chem. Phys.*, 1970, **53**, 1126–1130.

65 A. C. Ferrari, J. Robertson, *Phys. Rev. B*, 2000, **61**, 14095.

66 M. W. Barsoum, T. El-Raghy, L. Farber, M. Amer, R. Christini, A. Adams, *J. Electrochem. Soc.*, 1999, **146**, 3919–3923.

67 M. Naguib, V. Presser, D. Tallman, J. Lu, L. Hultman, Y. Gogotsi, M.W. Barsoum, *J. Am. Ceram. Soc.*, 2011, **94**, 4556–4561.

68 Y. Yang, H. Wang, J. Zhang, R. Zhao, Y. Liang, Q. Jiang, *J. Am. Ceram. Soc.*, 2008, **91**, 2736-2739.

69 Y. G. Zainulin, S. I. Alyamovsky, G. P. Shveikin, *J. Phys. Chem. Solids*, **1978**, 39, 29-31.

Effect of different environments on oxidation of Ti_3C_2 MXene structures is investigated using ReaxFF molecular dynamics simulations and experimental techniques.